J Mater Sci: Mater Med (2011) 22:2175–2185
DOI 10.1007/s10856-011-4412-6

The influence of silicon substitution on the properties of spherical- and whisker-like biphasic α-calcium-phosphate/ hydroxyapatite particles

B. Jokic · M. Mitric · M. Popovic · L. Sima · S. M. Petrescu · R. Petrovic · Dj. Janackovic

Received: 28 April 2011 / Accepted: 28 July 2011 / Published online: 7 August 2011

Abstract In this work, the influence of the morphology of hydroxyapatite particles on silicon substitution through hydrothermal synthesis performed under the same conditions was investigated. Spherical- and whisker-like hydroxyapatite particles were obtained starting from calcium-nitrate, sodium dihydrogen phosphate, disodium-ethylenediaminetetraacetic acid and urea (used only for the synthesis of whisker-like particles) dissolved in aqueous solutions. Silicon was introduced into the solution using tetraethylorthosilicate. X-ray diffraction, infrared spectroscopy, scanning electron microscopy, energy-dispersive X-ray spectroscopy and transmission electron microscopy indicate that silicon doping induce different phase compositions and bioactivity of spherical- and whisker-like hydroxyapatite particles obtained under the same hydrothermal conditions. Silicon-substituted, spherical hydroxyapatites particles showed greater phase transformation to silicon-substituted α-calcium-phosphate compared with whiskers-like hydroxyapatite particles synthesized with the same amount of added silicon. Metabolic activity assay performed with SaOs2 osteosarcoma cells showed better biocompatibility of annealed biphasic spherical-like particles compared with annealed whiskerlike particles while dried spherical-like particles induce high cytotoxicity effect.

B. Jokic (✉) · R. Petrovic · Dj. Janackovic
Faculty of Technology and Metallurgy, Karnegijeva 4, 11000 Belgrade, Serbia
e-mail: bjokic@tmf.bg.ac.rs; jokicb@yahoo.com

M. Mitric · M. Popovic
Institute of Nuclear Science "Vinca", P.O. Box 522, 11001 Belgrade, Serbia

L. Sima · S. M. Petrescu
Institute of Biochemistry, Romanian Academy, Splaiul Independentei 296, 060031 Bucharest, Romania

1 Introduction

Hydroxyapatite [$Ca_{10}(PO_4)_6(OH)_2$, HA] is a well-known synthetic material which is used for bone replacement due to its chemical and crystallographic similarities with the inorganic components of bone and tooth [1]. HA is only one of a number of calcium-phosphorous (CP) compounds, such as octocalcium phosphate and both phases of tricalcium-phosphate ($Ca_3(PO_4)_2$ or α-TCP, β-TCP), which are biocompatible [2–6]. The apatite phase, which makes up the inorganic component of hard tissue, can be described as a multisubstituted calcium-phosphate apatite with different degrees of stoichiometry with the Ca/P ratio ranging from 1.55 to 2.2 and ionic substitutions, principally carbonate (up to 8 wt. %), making it more like an A–B-type carbonate-substituted apatite [3, 4]. Potential trace level substituent element include sodium (up to 0.8 wt%) and magnesium (up to 0.5 wt%), while ultra-trace level substituents include potassium, strontium, zinc, fluorine, chlorine and silicon (Si) [3, 7]. Although these levels of substitution are small, the different ions play a major role in the biochemistry of the hard tissue [8].

One way of improving the bioactive behavior of hydroxyapatite is to obtain substituted apatites with chemical compositions and structures that resemble the natural materials. These ionic substitutions can affect the surface structure and charge of hydroxyapatite, which could have an influence on the material in biological environments and invoke enhanced cell adhesion, differentiation and gene expression [9, 10]. In this sense, an interesting way to improve the bioactivity of hydroxyapatite is the

incorporation of silicon (or silicon groups) into the apatite structure, taken into account the influence of this element on the bioactivity of bioactive glasses and glass–ceramics [9].

Preliminary studies performed by Gibson et al. showed that the incorporation of silicon into the HA lattice resulted in enhanced bioactivity and induced structural changes, such as distortion of the lattice of HA, i.e., the *a* axis decreased and the *c* axis increased with increasing silicate content [11, 12]. Moreover, it was observed that the addition of Si during the synthesis of HA leads to an improvement of the bioactive behavior [13–15]. Numerous studies have demonstrated that ionic substitution can affect the surface structures and charge of HA, which could play an important role in cell adhesion and, subsequently, various cell behaviors, such as proliferation, migration, cytoskeletal arrangement and differentiation, rather than its composition [16, 17]. Several methods for the synthesis of silicon-substituted hydroxyapatites have been described, including the sol–gel method [18], hydrothermal synthesis [19], solid state reactions [20], and wet methods [21, 22]. Wei and Akin [23] studied zinc and silicon doping of TCPs with a constant (Zn + Ca)/(P + Si) ratio of 1.50, using fumed SiO_2 and ZnO as the source of Si and Zn ions, respectively, and found that silicon doping favored the formation of α-TCP while zinc doping favored the formation of β-TCP.

Langstaff et al. [24] and Sayer et al. [13] showed that firing CaP precipitates having a constant Ca/P ratio of 1.67 with added silica forms multiphase mixtures primarily composed of silicon-stabilized α-TCP (Si-α-TCP) in balance with HA and β-TCP. They concluded that a biphasic (Si-α-TCP/HA) composition with random dissolution generates the necessary environment to stimulate the activity of osteoclasts.

Although silicon substituting the phosphorus atoms in the hydroxyapatite lattice influences the bioactive behavior of the material, it is not clearly known whether silicon substitutes completely or partially the phosphorus in the hydroxyapatite structure or whether the silicon species remain as a separate phase in the material.

In this work, the aim was to study the incorporation of silica into apatite structure in order to enhance formation of silicon-stabilized α-TCP and improve a bioactivity compared with that of pure hydroxyapatite through a controlled crystallization process under hydrothermal conditions at high temperature. To accomplish this purpose, two synthesis procedures were used to obtain materials with controlled spherical- and whisker-like morphology and chemical composition, both of which are essential for the application of biphasic (HA/Si-α-TCP) material as a bioceramic. The influence of silicon substitution in spherical- and whisker-like particles on the structure, phase transformations and bioactivity of the obtained apatites was investigated under in vitro conditions.

2 Materials and methods

2.1 Sample preparation

The starting point of the synthesis of a silicon-substituted apatite (Si-HA) was the preparation of hydroxyapatite with two different morphologies (spherical- and whiskers-like, denoted as S and W, respectively in the further text) by the hydrothermal method using $Ca(NO_3)_2{\cdot}4H_2O$, $NaH_2PO_4{\cdot}2H_2O$, $Na_2H_2EDTA{\cdot}2H_2O$ (the last one was used for the synthesis of spherical-like particles) and urea as previous described [25, 26]. The appropriate quantities of the reactants were calculated to prepare stoichiometric hydroxyapatite (Ca/P = 1.67) and hydroxyapatite with Ca/P molar ration that approaches 1.50. The employed amounts of $Ca(NO_3)_2{\cdot}4H_2O$, $NaH_2PO_4{\cdot}2H_2O$, $Na_2H_2EDTA{\cdot}2H_2O$ and urea dissolved in 1,500 ml of distilled water are listed in Table 1.

The silicon-substituted apatites were prepared using a Ca/P molar ration that approaches 1.50 by adding two different amounts of tetraethyl orthosilicate (TEOS) as the source of silicon ions (Table 1). Each synthesis was performed by mixing $Ca(NO_3)_2{\cdot}4H_2O$, $NaH_2PO_4{\cdot}2H_2O$,

Table 1 Quantities of reactants used for the synthesis of the different HA and Si-HA samples

Sample	$Ca(NO_3)_2{\cdot}4H_2O$ (mol)	$NaH_2PO_4{\cdot}2H_2O$ (mol)	$Na_2H_2EDTA{\cdot}2H_2O$ (mol)	Urea (mol)	TEOS (mol)	Ca/P (molar)
S1.67	0.0642	0.0385	0.0199	0.2000	0	1.67
S1.50	0.0577	0.0385	0.0199	0.2000	0	1.50
S1.50SiL	0.0577	0.0385	0.0199	0.2000	0.0024	1.50
S1.50SiH	0.0577	0.0385	0.0199	0.2000	0.0240	1.50
W1.67	0.0642	0.0385	0	0.2000	0	1.67
W1.50	0.0577	0.0385	0	0.2000	0	1.50
W1.50SiL	0.0577	0.0385	0	0.2000	0.0024	1.50
W1.50SiH	0.0577	0.0385	0	0.2000	0.0240	1.50

$Na_2H_2EDTA{\cdot}2H_2O$ (only for spherical-like HA particles) and urea in 1,500 ml of distilled water in a glass vessel. Different amount of TEOS (see Table 1) were first dissolved in 40 ml of absolute ethanol and then added to the main solutions. In order to provide uniform thermal transport, 1,500 ml of distilled water was placed in the gap between the glass vessel and the stainless-steel vessel. The autoclave was heated up to 160°C during 1 h and kept at this temperature for 2 h. After this period the autoclave was left to cool down slowly over 10 h to room temperature. The HA precipitates were collected from the solution by vacuum filtration and washed with distilled water. The synthesized products were heated, using a heating rate of 10°C min^{-1}, in an air atmosphere at 1,200°C for 2 h.

2.2 Characterization of the silicon doped and undoped HA powders

The diffraction patterns of the polycrystalline samples were measured using a conventional powder diffractometer (Ital Structures APD 2000) with Bragg–Brentano geometry and $CuK_{\alpha 1,2}$ radiation (Ni filter). XRD plots were recorded at room temperature in the 2θ range 5–70° with a 0.02° 2θ step and a 2 s counting time per data point. A 1/2° source slit and 0.1 mm receiving slit were used. Phase identification, profile analysis and lattice parameters refinement were accomplished using the WinPLOTR [27] and PowderCell [28] programs. The starting parameters in refinement analysis were taken from Kay et al. [29] and Smith et al. [30].

The morphology of the obtained powders was studied by scanning electron microscopy (SEM) JEOL JSM-5800 at 20 kV and transmission electron microscopy (TEM) JEOL T-100. Prior to the SEM analysis, the powder samples were coated with gold using a spatter coater, while for TEM, the samples were dispersed in ethanol and deposited on a Cu grid.

The chemical composition of the samples was analyzed using an Energy Dispersive Spectrometer (EDS) Isis 3.2, with a SiLi X-ray detector (Oxford Instruments, UK) connected to the scanning electron microscope and a computer multi-channel analyzer, and Energy Dispersive X-ray Fluorescence Spectroscopy (EDXRF) using Oxford ED 2000 spectrometer (Oxford Instrument, UK).

Fourier transform infrared (FTIR) spectroscopy was performed using a Bomem MB 100 Hartmann and Braun spectrometer in the wavenumber range from 400 to 4,000 cm^{-1}. The crystalline products ($\approx$3 mg) were thoroughly ground with ($\approx$500 mg) potassium bromide powder (KBr for IR, Merck) in an agate mortar to homogenize the mixture.

The presence of EDTA in powder samples was determined using liquid chromatography–tandem mass spectrometry (LC–MS/MS) method. The extracts of powder samples were analysed by Surveyor LC system (Thermo Fisher Scientific, Waltham, MA, USA) equipped with Zorbax Eclipse® XDB-C18 column, 4.6 mm × 75 mm i.d. and 3.5 μm particle size (Agilent Technologies, Santa Clara, CA, USA). The mobile phase consisted of 40% water and 60% methanol with the flow rate of 0.5 ml min^{-1}. Mass spectra were obtained by LCQ Advantage (Thermo Fisher Scientific, Waltham, MA, USA) quadrupole ion trap mass spectrometer. Electrospray ionization technique was used. Analyte was analyzed in the negative ionization mode with the optimal source working parameters as follows: source voltage (4.5 kV), sheath gas (23 au, i.e. 23 arbitrary units) and capillary temperature (290°C).

2.3 Cell culture and cell seeding

Experiments were performed with SaOs2 osteosarcoma cells, which were cultured in McCoy medium (Sigma) supplemented with 10% fetal calf serum FCS (Biochrom AG), Glutamax and Pen/Strep (Gibco) and kept at 37°C in 5% CO_2 humid atmosphere in a Heraeus incubator. All the tested materials were sterilized in water vapor at 121°C for 30 min in a Falcon 30 Autoclave (LTE Scientific) prior to cell culture.

2.4 Metabolic activity assay

The same approaches for the quantification potential cytotoxicity of biomaterials were followed for the dried and annealed spherical- and whiskers-like samples. The dried (at 100°C for 2 h) and annealed (at 1,200°C for 2 h) powder samples were extracted in complete media (0.2 g ml^{-1}) for 24 h prior to addition in triplicate onto the bone cell monolayers cultivated in a 96-well culture dish (TPP). After incubation for 72 h, the cell viability was rested using a CellTiter 96® AQueous One Solution Cell Proliferation Assay kit following the manufacturer's instructions (Promega). The optical density (450 nm) was read using a Mithras spectrofluorometer (Berthold) for both samples and controls. Duplicate samples were tested for each type of material.

2.5 In vitro assay in simulated body fluid (SBF)

The synthesized silicon-doped and undoped powders annealed at 1,200°C (0.5 g) were immersed in 30 ml of SBF, with an ionic concentration and pH nearly equal to those of human plasma, at 37°C for 72 h [31]. After immersion, the samples were dried and sputtered with Au–Pd alloy for SEM observation.

3 Results and discussion

The XRD patterns of the precipitated HA powders are shown in Fig. 1. The patterns of the raw spherical- and whiskers-like powders were characteristic of crystalline apatite according ICDD standard for HA (PDF 9-432). The samples S1.67, S1.50, S1.50SiL and S1.50SiH dried at 105°C exhibited poorly resolved diffractograms which corresponded to those of biological apatite [3]. However, it can be observed that the patterns for the W1.67, W1.50, W1.50SiL and W1.50SiH samples, due to a strong preferential crystallite orientation (Fig. 1), were significantly different to the usually obtained patterns of HA with a random crystallite orientation [26, 32–34]. In addition, as can be observed on the diffractogram for the samples W1.67, W1.50, W1.50SiL and W1.50SiH (Fig. 1), very intensive reflections arose from a plane close to the 100 direction, which masked the reflections along the 001 direction. Furthermore, evidence that the half width at half maximum of the peaks on the diffractograms were not significantly changed from those of crystal systems in which the crystallites were developed along the c axis, indicates that the crystallites had the similar dimensions in all directions. The refined unit cell parameters of the crystallized powders are listed in Table 2. With increasing expected silicon content in apatite structure an increase of the *a* and *c* parameters can be seen for the spherical-like particles, and an increase of the *a* and *c* parameters for the whiskers-like particles with Ca/P = 1.50, which can be taken as evidence of the incorporation of SiO_4^{4-} into the lattice thereby replacing PO_4^{3-} anions. The discrepancy between the lattice parameters for saturated Si-TCP found by Sayer [13] and the lattice parameters determined in this work are not surprising because of the different synthesis conditions and the silicon content, suggesting differences in chemical composition with respect to silicon-substituted apatites obtained by the precipitation and solid state methods.

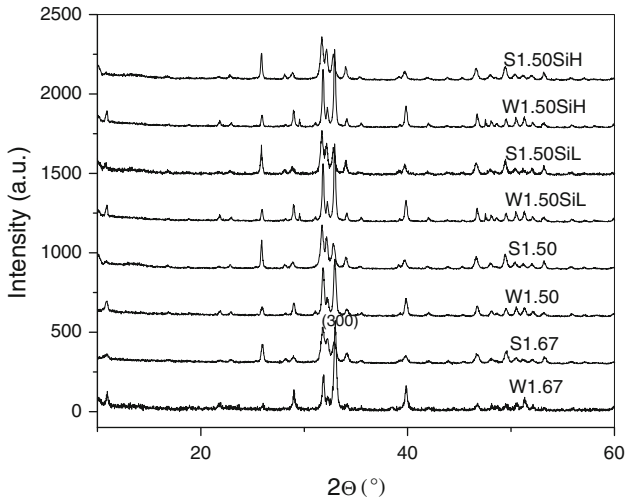

Fig. 1 X-Ray diffractograms collected from the hydrothermal synthesized products dried at 105°C. Reflection marked as 300 correspond to 100 direction

It should be noted that X-ray diffraction analysis of an as-synthesized apatite powder can result in a diffraction pattern that can resemble HA even though the Ca/P is different than the stoichiometric molar ratio of 1.67 for HA. For this reason X-ray diffraction analysis is performed on samples that have been calcinated at temperatures higher than 800°C in order to determinate the effect of chemical changes on the phase composition and structure of hydroxyapatite [35, 36].

FTIR spectroscopy was used to study the as-prepared powders and heat-treated powders in order to quantify the effect of the silicon substitution on the different functional groups, such as hydroxyl and phosphate groups, of the hydroxyapatite. The FTIR spectra of the as-prepared S1.67, S1.50, S1.50SiL, S1.50SiH, W1.67, W1.50, W1.50SiL and W1.50SiH are shown in Fig. 2. The intensity of the liberation OH band was increase in the spectra of the S1.67, S1.50, S1.50SiL and S1.50SiH samples. The spectra of all the as-prepared samples were found to be very similar. A weak OH band at 3,569 cm^{-1} is partially obscured by a broad band in the wavenumber range 2,600–3,700 cm^{-1}, which is characteristic of moisture in the sample. The three peaks at 1100, 1040, and 960 cm^{-1} arising from $\nu 3$ and $\nu 1$ bands and the two peaks at 605 and 567 cm^{-1} arising from the $\nu 4$ band were identified in the all the spectra. The carbonate $\nu 3$ band, as three peaks at 1635, 1460 and 1,416 cm^{-1}, and the carbonate $\nu 2$ band, as a single peak at 875 cm^{-1}, were found for all the as-prepared samples. It can be observed that peaks belonging to the carbonate $\nu 3$ band at 1,635 and 1,415 cm^{-1} for the as-prepared W1.67, W1.50, W1.50SiL and W1.50SiH samples were slightly shifted to 1,622 and 1,409 cm^{-1} for the as-prepared S1.67,

Table 2 The refined lattice parameters of the synthesized powders

Lattice	Sample							
	S1.67	S1.50	S1.50SiL	S1.50SiH	W1.67	W1.50	W1.50SiL	W1.50SiH
a (Å)	9.4498(3)	9.4669(3)	9.4683(3)	9.4693(3)	9.4442(3)	9.4377(3)	9.4412(3)	9.4522(3)
c (Å)	6.8881(2)	6.8997(2)	6.9026(2)	6.9027(2)	6.8913(2)	6.8921(2)	6.8939(2)	6.9022(2)

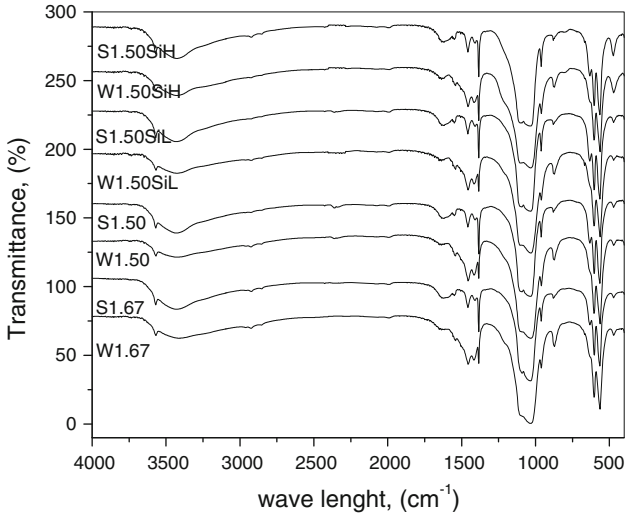

Fig. 2 IR spectra of the hydrothermally synthesized products dried at 105°C

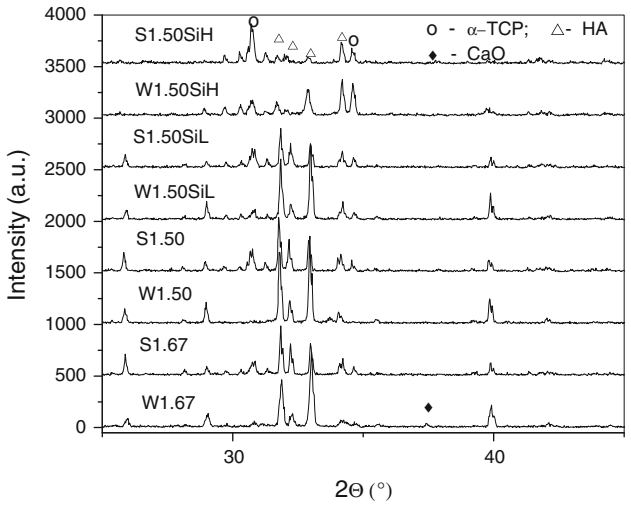

Fig. 3 X-Ray diffractograms of the hydrothermally synthesized products after annealing at 1,200°C for 2 h

S1.50, S1.50SiL, S1.50SiH samples. A slight shifting was observed for the carbonate $\nu 2$ band; from 875 cm^{-1} for the W1.67, W1.50, W1.50SiL and W1.50SiH samples to 880 cm^{-1} for the S1.67, S1.50, S1.50SiL and S1.50SiH samples. A well-resolved peak at 1,140 cm^{-1}, characteristic of the Si–O bond, could not be observed in the FTIR spectra.

X-ray diffraction patterns of the samples heat-treated at 1,200°C for 2 h are shown in Fig. 3. The patterns of the two hydroxyapatite materials spherical-like and whisker-like morphology appeared to behave differently during heating, with different amounts of HA and α-TCP phases detected. All the diffraction peaks matched the ICDD (JCPDS) standard for HA (PDF Card No. 9-432, whereas the Si-α-TCP phase resembled the crystallography of α-TCP (PDF Card No. 9-348). Comparing the diffractograms of spherical- and whisker like apatite synthesized from solutions with different starting Ca/P molar ratios; 1.67 (sample S1.67 and W1.67) and 1.50 (sample S1.50 and W1.50), the Ca/P ratio has a direct effect on the phase composition. Slightly pronounced phase transformation from HA to α-TCP can be observed in the diffractogram of the S1.50 compared to the S1.67. Analyzing the diffractograms of the W1.50 and W1.67 samples, it can be seen that particles with a whisker-like morphology were more stable during heating at 1,200°C than the spherical-like S1.50 and S1.67 samples. On the diffractogram of the W1.67 sample small amount of CaO phase (PDF Card No. 82-1690) can be observed. Analyzing the diffracogram of the spherical-like particles (Fig. 3), the S1.5SiH sample doped with a ten times higher amount of silicon shows the presence of α-TCP with the residual amount being HA phase, while on the diffractogram of the W1.50SiH sample, it can be seen that almost equal amounts of α-TCP and HA phase are present. Significantly, no calcium silicate peaks were identified on the diffractograms, suggesting that Si forms a substituted or disperse phase within the phosphate lattice. According to these results, the formation of the Si-α-TCP phase can be explained through the crystallography of the calcium phosphate system induced defect chemistry associated with silicon substitution into the calcium phosphate lattice. The changes in the synthesis conditions could result in silicon substitution at different site and by a different charge compensation mechanism.

The FTIR spectra of the 2 h heat-treated at 1,200°C samples, S1.67, S1.50, S1.50SiL, S1.50SiH, W1.67, W1.50, W1.50SiL and W1.50SiH, are shown in Fig. 4.

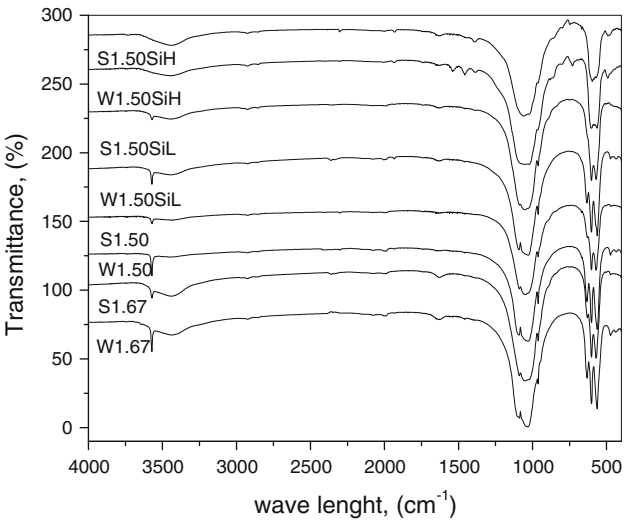

Fig. 4 IR spectra of the hydrothermally synthesized products annealed at 1,200°C for 2 h

There are several significant changes from the as-prepared samples (see Fig. 3). The broad band caused by moisture in the sample had almost completely disappeared and the OH band in the heat-treated samples appeared as a very sharp peak, except for the S1.50SiH and W1.50SiH samples, in the spectra of which both the OH stretching mode peak at 3,575 cm^{-1} and the broad band caused by moisture were completely absent. The disappearance of the OH peaks indicates that OH vacancies were formed in the HA lattice to compensate for the charge defect induced by substitutions of Si^{4+} at P^{5+} sites. The clear peaks that corresponded to carbonate at 1635, 1460, 1416 and 875 cm^{-1} in the FTIR spectra of the as-prepared samples (Fig. 2) had disappeared after heat treatment at 1,200°C, except for in the FTIR spectra of the W1.67 and W1.50 samples, in which a small peak at 1,635 cm^{-1} was still visible. The most notable effect of silicon substitution was observed comparing the FTIR spectra of the as-prepared and heat-treated sample in the ranges of the PO_4 bands between 800 and 1,000 cm^{-1} and 450 and 700 cm^{-1}. The spectra of the heat-treated sample had the characteristic $\nu 3$ and $\nu 1$ bands at 1088, 1030, and 962 cm^{-1} and the $\nu 4$ band, identified by three peaks at 631, 604, and 560 cm^{-1}[37]. There were small shifts of the peak at 630 cm^{-1} in the spectra of the S1.67, S1.50 and S1.50SiL samples and of the peak at 633 cm^{-1} in the spectra of the W1.67, W1.50 and W1.50SiL samples. These peaks were not visible in the spectra of the S1.50SiH and W1.50SiH samples. It can be observed that the $\nu 4$ band of heat treated W1.67, W1.50 and W1.50SiL showed separated peaks at 563 and 573 cm^{-1}. Separation of the peaks at 565 cm^{-1} was not observed in the spectrum of the W1.50SiH sample. More significantly, additional peaks at 945 cm^{-1} for all heat-treated samples, peaks at 890 cm^{-1} for the S1.67, S1.50 and S1.50SiL sample and peaks at 860, 800, 730 and 493 cm^{-1} for the S1.50SiH and W1.50SiH samples were observed. The band at 800 cm^{-1} has been associated with an O–Si–O band [38].

The micrographs of the non-agglomerated spherical particles and whisker-like particles obtained by a hydrothermal method are shown in Fig. 5. It could be seen that the size of the spherical particles were in the range of 1 to 3 μm, while the whisker-like particles were up to 150 μm long and did not have narrow size distribution as consequence of preferential crystal growth along one axis [26, 32, 33]. The hollow spherical particles (Fig. 5a, c and e) consist of a large number of aggregated rod-like nanoparticles of size between 200 and 500 nm (Fig. 5a inset) depending of spherical particle diameter. It can be observed that the surface of the spherical particles was less rough when the higher amount of silicon was added into the system (insets in Fig. 5a, c and e), which was induced by the nanosize silicon particles that were formed on the top of the rod-like crystallites (inset in Fig. 5e) of which the spherical particles are composed. Formation of the nanosize silicon particles is more visible on the whiskers-like particles synthesized under the same hydrothermal conditions but without the addition of Na_2EDTA to the starting solution (Fig. 5f). In the micrograph of the whisker-like particles synthesized with the smaller amount of silicon, the formation of nanosize silicon on the flat surface of the whiskers can not be observed (Fig. 5d). Attendance of Si nanoparticles formed at the surface of spherical- and whiskers-like particles, S1.50SiL and W1.50SiL samples is a consequence of low concentration of Si-ions in starting solution.

Nanosilicate particles are formed by hydrolyzing monomeric TEOS precursors in the presence of base (NH_3) as catalyst, the concentration of which are increased through urea decomposition. As TEOS and water are immiscible, ethanol was used as a homogenizing agent in the starting solution, in which further ethanol is produced as a by-product of the hydrolyze reaction. According to Iler, the condensation of monomers occurs in such a fashion as to maximize the number of Si–O–Si bonds and minimize the number of terminal hydroxyl groups through internal condensation, thereby creating three dimensional particles. These particles further condense to the most compact state with OH residual groups on the outside and serve as nuclei [39]. At or above pH 7, both the solubility and dissolution rates of silica are maximized and because the silica particles are appreciably ionized above this pH value, particle growth occurs without aggregation or gelation [39]. Formation of nanosilicate particles on the surface of hydroxyapatite particles could be explained according above mentioned mechanisam, because almost the same conditions are present during synthesis. Further growth is by the Ostwald ripening mechanism, whereby larger particles grow on account of the highly soluble small particles, which is additionally enhanced at the higher temperatures that exist under hydrothermal conditions. It can be observed in Fig. 5f and 6d that the size of the spherical silica particles formed on the surface of the spherical- and whisker-like particles was about 50 nm.

There are typically two coating mechanism that can occur during synthesis based on heterogeneous nucleation phenomena (surface nucleation) and heterocoagulation processes. The surface nucleation occurs via the adsorption of partially hydrolyzed TEOS molecules onto the hydroxyapatite surface where under basic conditions, the silanol groups react with each other forming siloxane bonds. The heterocoagulations mechanism proceeds via the adsorption on the hydroxyapatite surface of silica particles previously nucleated in solution. It could be presumed that the surface mechanism was the dominant mechanism for the S1.50SiH and W1.50SiH samples due to the basic

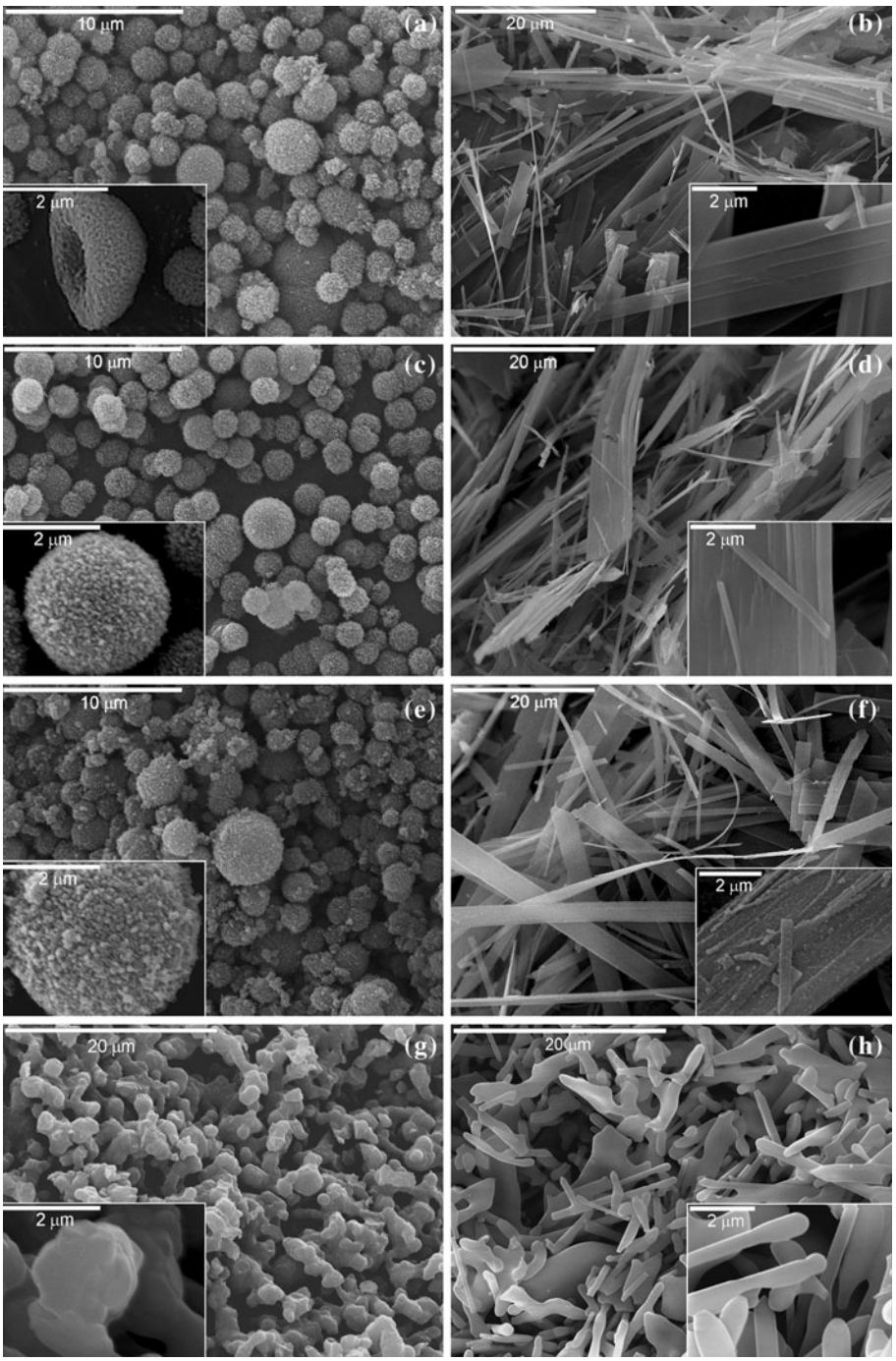

Fig. 5 SEM micrographs of hydrothermally prepared samples with high magnification *insets*: **a** S1.50, **b** W1.50, **c** S1.50SiL, **d** W1.50SiL, **e** S1.50SiH, **f** W1.5SiH, **g** S1.50SiH annealed at 1,200°C and **h** W1.50SiH annealed at 1,200°C

conditions induced by urea decomposition and the low TEOS concentration [40].

Transmission electron microscopy was applied to investigate the microstructure of the spherical- and whiskers-like particles (Fig. 6). A low magnification, the TEM image of the dried SHA05 sample (Fig. 6a) shows that the spherical particles were formed from rod-like primary crystallites. The polycrystalline structure of the spherical particles doped with a small amount of silicon was confirmed by the diffraction pattern shown in the inset of Fig. 6a. In Fig. 6c (sample S1.50SiH), the presence of spherical nano-size silica particles that are formed on the surface of the main particles can be observed. It turns out that the crystallinity of the sample was less pronounced, which was affected by the presence of silica nano-particles (inset of Fig. 6c). In the micrograph of sample W1.50SiL (Fig. 6b), the presence of silica particles on the surface of the whiskers was not observed and the microdiffraction pattern (inset of Fig. 6b) reveals the crystalline structure of the sample. Synthesis of whiskers doped with a ten times

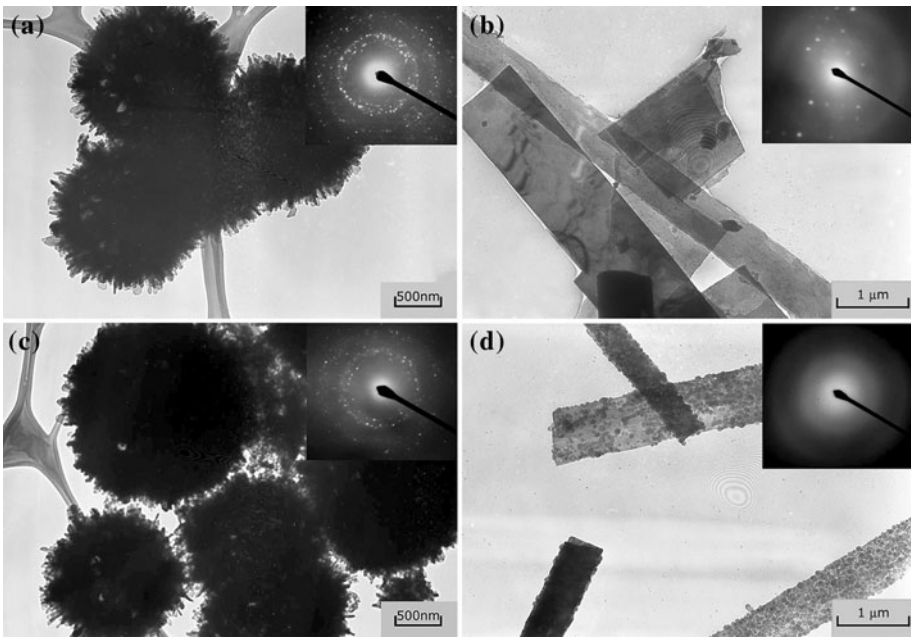

Fig. 6 TEM micrographs of hydrothermally prepared samples with electron diffraction *insets*: **a** S1.50SiL, **b** W1.50SiL, **c** S1.50SiH and **d** W1.50SiH

higher concentration of silicon (Fig. 6d) leads to the formation of ninosize silica particles that evenly cover the surface of the whiskers. The diffuse diffraction pattern corresponding to the centre of the whiskers (shown in Fig. 6d) indicates the amorphous structure of the formed silica nano-particles.

With the view of assessing the potential cytotoxicity of the synthesized spherical- and whisker-like HA, the proliferation of SaOs2 cells in the presence of HA powder extracts was first determined. The MTS assay, Fig. 8, shows the number of adherent cells cultured in 3 days on extract of spherical- and whiskers-like silicon doped and undoped powders with various nanostructures. The data show that the dried spherical particles doped and undoped with silicon were toxic for the cells, while the dried whiskers-like particles did not show this effect under the same conditions. This effect was prevented by annealing the spherical HA powders at 1,200°C (Fig. 5g and h). Moreover, annealing at 1,200°C improved the biocompatibility of all the synthesized HA powders, with the exception of W1.50SiH, probably induced the Si level in the fluid to over the physiology range and optimum level of Si required to achieve the most favorable biological response to a calcium-phosphate bone graft substitute [41–43].

It can be seen that the spherical- and whiskers-like particles doped with the smaller amount of silica showed the best bioactivity compared with same undoped particles and the particles doped with the higher amount of silicon. Although, there is no difference in phase composition between undpoed and doped in low concentration powder samples heated at high temperature, higher proliferation of SaOs2 cells in powder extracts of S1.50SiL and W1.50SiL is evident. EDS analysis was not detect presence of Si in dried S1.50SiL and W1.50SiL samples because small amount of Si substituted in crystal structure of HA and low detection limit of this analysis technique. Chemical analysis performed by EDXRF spectroscopy was shown presence of silicon in a small amount in the S1.50SiL and W1.50SiL samples (see Table 3). According to the obtained results, the powders doped with small amount of silicon posses higher in vitro bioactivity than silicon-free hydroxyapatite. This indicate that Si substitution in small amount do not significantly affect phase transformation in α-TCP but has great influence on cell proliferation. Appreciably higher concentration of silicon measured in samples S1.50SiH and W1.50SiH has negative effect on cell proliferation. This is in accordance with a previously published results where silicon substitution with 0.8 wt% being the optimum concentration for cell adhesion [44]. Comparing the results obtained from the MTS assay (Fig. 7), the silicon-doped spherical particles S1.50SiL annealed at 1,200°C seemed the optimal for cell proliferation.

Table 3 Silicon content measured by EDXRF

Sample	S1.50SiL	S1.50SiH	W1.50SiL	W1.50SiH
Si, wt%	0.55(3)	2.10(3)	0.58(3)	2.73(3)

One reason that explain different bioactivity of powder extracts could be the different phase composition of the samples after annealing at 1,200°C and higher solubility of α-TCP phase that induces better cells activity [45, 46]. Different bioactivity in spherical- and whiskers-like

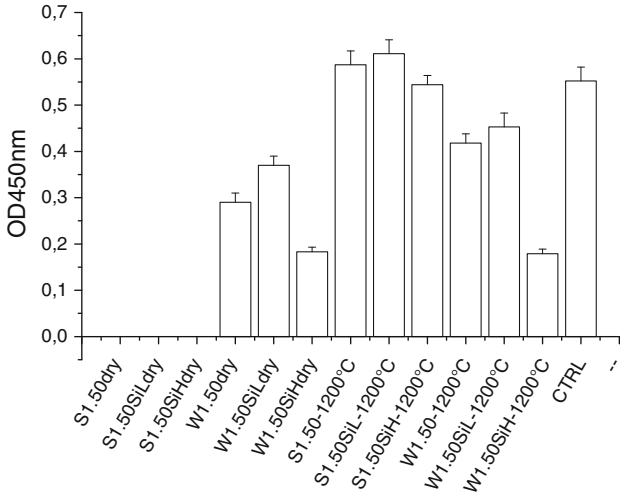

Fig. 7 MTS assay performed on SaOs2 osteosarcoma cells after 72 h treatment with spherical- (S) and whisker-like (W) powders extracts

powder extracts probably lies in a fact that silicon substitution is not occurred at the same amount into the cristal structure of spherical- and whisker-like particles. It was observed that powder extracts of dried spherical particles exhibit high cytotoxicity effect on SaOs2 cell proliferation. After a chemical analysis performed on powder extracts using liquid chromatography–tandem mass spectrometry presence of residual EDTA was confirmed only in dried spherical-like particles in concentration of 65, 68 and 72 ppm for S1.50, S1.50SiL, and S1.50Sih sample, respectively. According to the previous studies in which EDTA salt was found to be toxic in vitro, presence of residual EDTA detected in extract of the dried spherical-like particles is probably responsible for high cytotoxicity effect on SaOs2 cells [47].

The micrographs of non-agglomerated spherical-like particles and whisker like particles annealed at 1,200°C for 2 h after immersion in SBF for 3 days are shown in Fig 8. The formation of a new hydroxyapatite phase precipitated during immersion in SBF is visible on the surfaces of all the samples. It can be seen that there are some difference in a degree of hydroxyapatite phase formed on the surface of silicon-doped and undoped spherical- and whisker-like particles tah is probably induced by different charge surface. Namely, on the micrographs of undoped spherical- and whisker-like particles (Fig. 8a and b), partial coverage of the surface with precipitated hydroxyapatite can be observed. A better surface coverage with a dense net of nanosized hydroxyapatite particles can be distinguished on the samples S1.50SiL and W1.50SiL (Fig. 8c and d) doped with the smaller amount of silicon. A denser and more uniform structure of precipitated hydroxyapatite is observed on the surface of the spherical particles (sample S1.50SiL) with the higher silicon content (Fig. 8e). The micrographs of the whiskers doped with the higher amount of silicon (Fig. 8f) show a somewhat different structure of the hydroxyapatite coat that covers the surface of the whiskers in comparison to the hydroxyapatite that were formed on the surface of the spherical particles synthesized with the same amount of silicon in the starting solution. The difference in the morphology of the HA particles and the surface coverage of the W1.50SiL sample is more marked compared with the difference between that formed on the S1.50 and W1.50SiL samples. The needles of hydroxyapatite formed on the surface of the S1.50SiH samples were smaller and disconnected, and the crudeness arrays on the surface were still visible (Fig. 8f). Difference in surface morphology observed at the annealed samples after immersion in SBF for 72 h indicate how a degree of silicon substitution affect formation apatite phase on the surface.

4 Conclusions

Silicon substituted hydroxyapatite with two different morphologies were prepared by the hydrothermal method. The hydrolysis of TEOS under basic conditions achieved through the gradual decomposition of urea under hydrothermal conditions at a high temperature. The investigations showed diverse silicon substitution under the same synthesis conditions on spherical- and whisker-like particles confirmed by XRD and EDXRF analyses, where small amount of added silicon enhance phase transformation from HA to α-TCP at lower temperature. These transformation are more pronounced on spherical-like particles. It was observed that a complete coating of the hydroxyapatite particles with nanosize silica was formed at the higher silica concentration, while at the lower concentration of silica, only substitution of phosphorous atoms in hydroxyapatite crystal lattice occurred; this was observed for both spherical- an whisker-like particles. According to the obtained results, the powders doped with small amount of silicon (0.55 and 0.58 wt% for S1.50SiL and W1.50SiL sample, respectively) posses higher in vitro bioactivity than silicon-free hydroxyapatite. Although, there is no significant difference in phase composition between undoped and doped in low concentration, dried and heated at high temperature powder samples, higher proliferation of SaOs2 cells in powder extracts of S1.50SiL and W1.50SiL is evident. This indicate that Si substitution in small amount do not affect phase transformation of HA in α-TCP but has great influence on cell proliferation. Appreciably higher concentration of silicon measured in samples S1.50SiH and W1.50SiH has negative effect on cell proliferation. This is in accordance with a previously published results where silicon substitution with 0.8 wt% being the optimum concentration for cell adhesion.

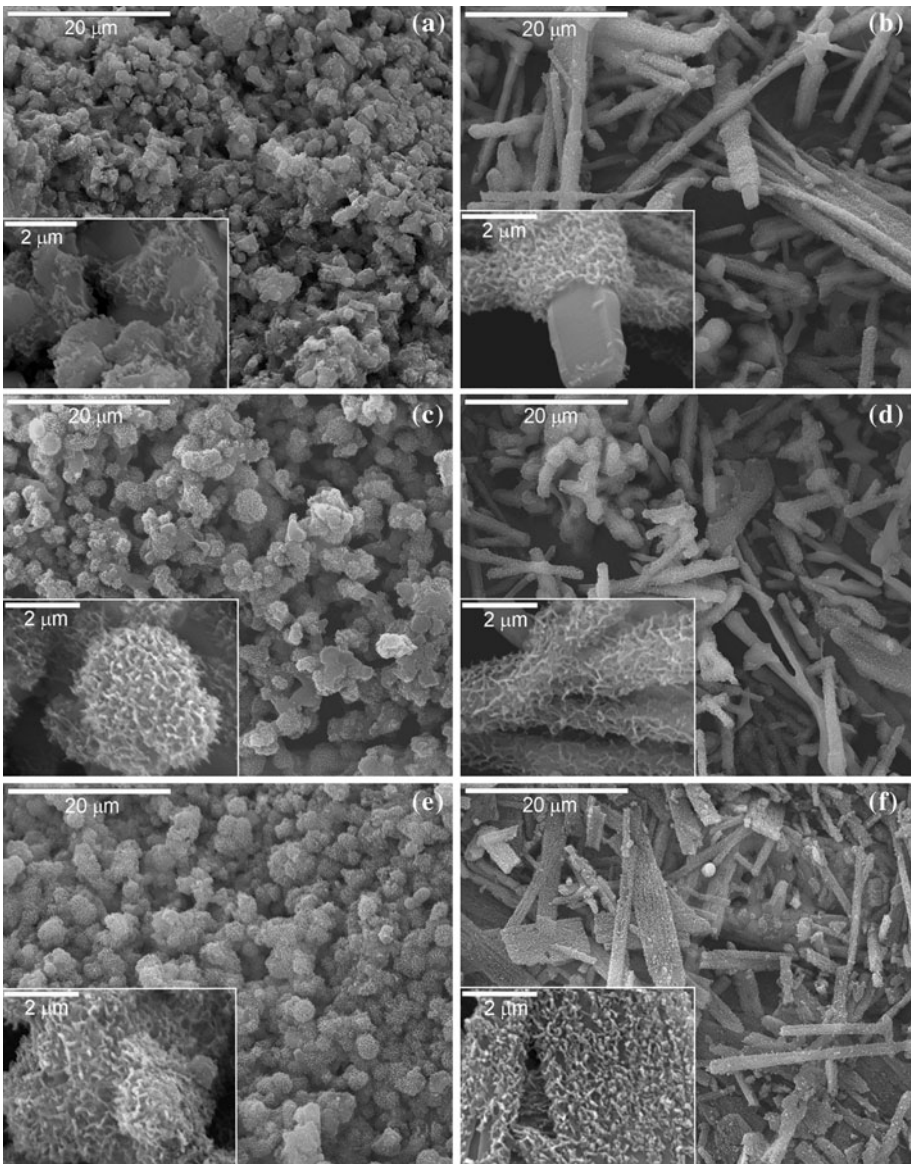

Fig. 8 SEM micrographs of hydrothermally prepared samples with high magnification insets after immersion in SBF for 72 h: **a** S1.50, **b** W1.50, **c** S1.50SiL, **d** W1.50SiL, **e** S1.50SiH, **f** W1.5SiH

The influence of phase and chemical composition can explain the considerably better bioactivity obtained on powder extracts of the spherical-like particles compared with whisker-like particles after annealing at higher temperatures. It was observed that powder extracts of dried spherical particles exhibit high cytotoxicity effect on SaOs2 cells induced by residual EDTA present only in dried spherical-like particles. It is evident that the amount of added silicon plays a fundamental role in the process of bioactivity and the surface chemistry.

Acknowledgments The authors wish to acknowledge the financial support from Ministry of Science and Technological Development Project No. III45019. We thank Dr. Karine Anselme for providing us the SaOs2 osteosarcoma cell line.

References

1. Bohner M. Calcium orthophosphates in medicine: from ceramics to calcium phosphate cements. Injury. 2000;31:37–47.
2. Kikawa T, Kashimoto O, Imaizumi H, Kokubun S, Suzuki O. Intramembranous bone tissue response to biodegradable octacalcium phosphate implant. Acta Biomater. 2009;5:1756–66.
3. Elliot JC. Structure and chemistry of the apatites and other calcium orthophosphates. Studies in Inorganic Chemistry. Amsterdam: Elsevier; 1994.
4. Dorozhkin SV. Calcium orthophosphates. J Mater Sci. 2007;42:1061–95.
5. Best SM, Porter AE, Thian ES, Huang J. Bioceramics: Past, present and for the future. J Eur Ceram Soci. 2008;28:1319–27.
6. Ferandez E, Gil FJ, Ginebra MP, Driessens FCM, Planell JA, Best SM. Calcium phosphate bone cements for clinical applications. Part I: Solution chemistry. J Mater Sci: Mater Med. 1999;10:169–76.

7. Racquel Z, LeGeros JP. Dense hydroxyapatite. In: Hench LL, Wilson J, editors. An Introduction to Bioceramics. Singapore: Word Scientific; 1993. p. 139–80.
8. Yamada MO, Tohno Y, Tohno S, Utsumi M, Moriwake Y, Yamada G. Silicon compatible with the height of human vertebral column. Biol Trace Elem Res. 2003;95:113–21.
9. Webster TJ, Massa-Schlueter EA, Smith JL, Slamovich EB. Osteoblast response to hydroxyapatite doped with divalent and trivalent cations. Biomaterials. 2004;25:2111–21.
10. Jell G, Stevens MM. Gene activation by bioactive glasses. J Mater Sci Mater Med. 2006;17:997–1002.
11. Gibson IR, Best SM, Bonfield W. Chemical characterization of silicon- substituted hydroxyapatite J. Biomed Mat Res. 1999;44:422–8.
12. Arcos D, Rodrı′guez-Carvajal J, Vallet-Regi M. Silicon Incorporation in Hydroxylapatite Obtained by Controlled Crystallization. Chem Mater. 2004;16:2300–8.
13. Sayer M, Stratilatov AD, Reid J, Calderin L, Stott MJ, Yin X, MacKenzie M, Smith TJN, Hendry AJ, Langstaff SD. Structure and composition of silicon-stabilized tricalcium phosphate. Biomaterials. 2003;24:369–82.
14. Balas F, Pérez-Pariente J, Vallet-Regí M. In vitro bioactivity of silicon-substituted hydroxyapatites. J Biomed Mater Res. 2003;66A:364–75.
15. Anselme K. Osteoblast adhesion on biomaterials. Biomaterials. 2000;21:667–81.
16. Thian ES, Huang J, Best SM, Barber ZM, Brook A, Rushton N, Bonfield W. The response of osteoblasts to nanocrystalline silicon-substituted hydroxyapatite thin films. Biomaterials. 2006;27: 2692–8.
17. Davies JE., Surface characterization of biomaterials. In: Ratner BD, editor, Amsterdam; Elsevier: 1998. p 219-34.
18. Ruys AJ. Silicon-doped hydroxyapatite. J Aust Ceram Soc. 1993;29:71–80.
19. Tanizawa Y. Suzuki T. Effects of silicate ions on the formation and transformation of calcium phosphates in neutral aqueous solutions J Chem Soc Faraday Trans. 1995;91(19):3499–503.
20. Boyer L, Carpena J, Lacout JL. Synthesis of phosphate-silicate apatites at atmospheric pressure. Solid State Ionics. 1997;95: 121–9.
21. Gibson IR, Huang J, Best SM, Bonfield W. Enhanced In Vitro Cell Activity and Surface Apatite Layer Formation on Novel Silicon-Substituted Hydroxyapatites. Bioceramics. 1999;12: 191–4.
22. Aizawa M, Patel N, Porter AE, Best SM, Bonfield W. Syntheses of Silicon-Containing Apatite Fibres by a Homogeneous Precipitation Method and Their Characterization. Key Eng Mater. 2006;309–311:1129–32.
23. Wei X, Akinc M. Si, Zn-modified tricalcium phosphates: a Phase composition and crystal structure study. Key Eng Mater. 2005; 284–286:83–6.
24. Langstaff S, Sayer M, Smith TJN, Pugh SM, Hesp SAM, Thompson WT. Resorbable bioceramics based on stabilized calcium phosphates. Part I: rational design, sample preparation and material characterization, Biomaterials. 1999;20:1727–41.
25. Janackovic D, Petrovic-Prelevic I, Kostic-Gvozdenovic L, Petrovic R, Jokanovic V, Uskokovic D. Influence of synthesis parameters on the particle sizes of nanostructured calciumhydroxyapatite. Key Eng Mater. 2001;192–195:203–6.
26. Jokic B, Mitric M, Radmilovic V, Drmanic S, Petrovi R, Janackovic Dj. Synthesis and characterization of monetite and hydroxyapatite whiskers obtained by a hydrothermal method. Ceram Int. 2011;37:167–73.
27. Roisnel T, Rodriguez-Carvajal J. WinPLOTR, a Tool to Plot Powder Diffraction Patterns. France: Laboratoire Leon Brillouin (CEA-CNRS); 1998.
28. G. Nolze, W. Kraus, PowderCell 2.3 Program, BAM Berlin, 2000.
29. Kay MI, Young RA, Posner AS. Nature. 1964;204:1050–2.
30. de Wolff P. Technisch Physische Dienst, Delft, The Netherlands, ICDD Grant-in-Aid, PDF 09-0432.
31. Kokubo T, Takadama H. How useful is SBF in predicting in vivo bone bioactivity? Biomaterials. 2006;27:2907–15.
32. Aizawa M, Porter AE, Best SM, Bonfield W. Ultrastructural observation of single-crystal apatite fibres. Biomaterials. 2005;26:3427–33.
33. Aizawa M, Ueno H, Itatani K, Okada I. Syntheses of calcium-deficient apatite fibres by a homogeneous precipitation method and their characterizations. J Eur Ceram Soc. 2006;26:501–7.
34. Tas C. Molten salt synthesis of calcium hydroxyapatite whiskers. J Am Ceram Soc. 2001;84:295–300.
35. Gibson IR, Rehman IU, Best SM, Bonfield W. Characterisation of the transformation from Ca-deficient apatite to β-tricalcium phosphate. J Mat Sci Mater in Med. 2000;11:533–9.
36. Gibson IR, Best SM, Bonfield W. Chemical Characterisation of Silicon-substituted Hydroxyapatite. J Biomed Mat Res. 1999;44: 422–8.
37. Jillavenkatesa A, Condrate RA. The infrared and Raman spectra of α- and β-tricalcium phosphate $Ca(PO_4)_2$. Spectrosc Lett. 1998;31:1619–1634.
38. Hollenstein C, Howling AA, Courteille C, Magni D, Scholz SM, Kroesen GMW, Simons N, de Zeeuw W, Schwarzenbach W. Silicon oxide particle formation in RF plasmas investigated by infrared absorption spectroscopy and mass spectrometry. J Phys D Appl Phys. 1998;31:74–84.
39. Brinker CJ, Scherer GW. Sol-Gel Science: The Physics and Chemistry of Sol-Gel Processing. San Diego: Academic Press; 1990.
40. Borum L, Wilson O. Surface modification of hydroxyapatite.Part II.Silica. Biomaterials. 2003;24:3681–8.
41. Landi E, Uggeri J, Sprio S, Tampieri A, Guizzardi S. Human osteoblast behavior on as-synthesized SiO_4 and B-CO_3 co-substitu. J Biomed Mater Res Part A. 2010;94A:59–70.
42. Hing KA, Revell PA, Smith N, Buckland T. Effect of silicon level on rate, quality and progression of bone healing within silicate-substituted porous hydroxyapatite scaffolds. Biomaterials. 2006;27:5014–26.
43. Botelho CM, Brooks RA, Best SM, Lopes MA, Santos JD, Rushton N, Bonfield W. Human osteoblast response to silicon-substituted hydroxyapatite. J Biomed Mater Res Part A. 2006; 79A:723–30.
44. Zou S, Ireland D, Brooks RA, Rushton N, Best S. The effects of silicate ions on human osteoblast adhesion, proliferation, and differentiation. J Biomed Mater Res B Appl Biomater. 2009;90: 123–30.
45. Tuck L, Astala R, Reid JW, Sayer M, Stott MJ. Dissolution and re-crystallization processes in multiphase silicon stabilized tricalcium phosphate. J Mater Sci: Mater Med. 2008;19:917–27.
46. Mastrogiacoma M, Corsi A, Francioso E, Di Comite M, Monetti F, Scaglione S. Reconstruction of extensive long bone defects in sheep using resorbable biocermics based on silicon stabilized tricalcium phosphate. Tissue Eng. 2006;12:1261–73.
47. Ballal NV, Kundabala M, Bhat S, Rao N, Rao BS. A comparative in vitro evaluation of cytotoxic effects of EDTA and maleic acid: Root canal irrigants. Oral Surg Oral Med Oral Pathol Oral Radiol Endod. 2009;108:633–8.